ICAS 2020 SHANGHAI
International Council of the Aeronautical Sciences
32nd Congress of the International Council of the Aeronautical Sciences
September 6-10, 2021
Pudong Shangri-La, Shanghai, China

OPTIMAL DESIGN OF A NEXT GENERATION HIGH-LIFT REUSABLE RE-ENTRY VEHICLE

Andrea Aprovitola[1], Luigi Iuspa[1], Giuseppe Pezzella[1] & Antonio Viviani[1]

[1]Engineering Department, University of Campania "L. Vanvitelli". Aversa (CE). Italy

Abstract

Upcoming manned space missions and sub-orbital tourism are requiring a safe and affordable re-entry from space, also intended for a non-specifically trained crew. In the view of the above missions requirements, new re-entry technologies are currently being developed. The present paper summarises research activity by the authors to develop a conceptual configuration and a Phase-A focused activity for next generation of reusable high-lift vehicles. A multi-objective, multi-disciplinary optimization procedure, consistent with an assigned set of requirements and constraints is performed.
The conceptual configuration is then frozen, and Phase-A design is performed using high order fidelity methods to validate trade-offs between the objective functions and design variables. Computational Fluid Dynamics simulations in several specified way-points along with the re-entry trajectory are performed. The most favourable aerothermal loading environment (i.e., pressure and convective heat flux loads) is then determined performing a single objective optimization by finding the guidance law compatible with a rather constant heat flux. CFD computation are also performed at very low Mach numbers to address longitudinal stability margin.
Finally, the body flaps effects on spacecraft aerodynamics at landing conditions is also addressed.

Keywords: Reusable space vehicles; Re-entry aerodynamics; Hypersonic flow; Multidisciplinary design optimization (MDO).

1. Introduction

The enhanced operational capabilities required to the International Space Station (ISS) for the future Lunar missions and the upcoming Martian fly-by mission are currently favouring a re-design of Crew Return Vehicles (CRV). CRV are high performance reusable spacecrafts, which will replace capsules for crew rescue or re-entry from the ISS. Future CRV will be able to perform a safe, comfortable (i.e., with g-loads of unit order), and high turnaround re-entry on horizontal runway. For the same reason, sub-orbital space tourism will favour horizontal landings as only low g-loads can be tolerated to comply with high safety standards for civilian passengers.
To date mission requirements of CRV follow different criteria than those adopted for the Space Shuttle, which was conceived mainly for cargo transportation.) Next generation CRV are not designed to transport heavy payloads. Therefore, differently from Space Shuttle design, CRVs are not expected to face high-peak thermal loads during re-entry.
The different requirements have several implications on the design of CRV aeroshape. First, the significant weight reduction and the need to reduce the aerothermal loads during re-entry (e.g., improving the crew safety) allow the designers to study non conventional aeroshapes. Small-sized Blended Wing Body (BWB) aeroshapes can be designed with fuselage and wing seamlessly integrated in a delta-shaped planform ($L/D \approx 1$ and relatively small S_r/m ratio).
A specific Angle of Attack (AoA) modulation allows a more gradual conversion of spacecraft energy into heat by increasing the time of the re-entry flight. Increasing the flight time allows to reduce convective peak heat flux; thus at the same time gives the the possibility to customise the landing spot. However, a more gentle aerothermal environment allows adopting non-ablative heat-shields, exclusively cooled by thermal radiation (i.e., high emissivity thermal protection materials).

Consequently, the vehicle benefits of a short refurbishment time for a high turnaround mission rate.
As outlined, CRV design has to satisfy a complex picture which relates safety, operability, structural and aerodynamic constraints, cost reduction, and finally flight comfort [4]. However, appropriate engineering solutions in the high-speed regime reflect poorly aerodynamic performances at low-speed and even less at landing.
Recent examples of CRV prototypes in literature shown that design specifications (referenced to the entire mission) can be pursued if the vehicle shape is derived from a seamless, multi-purpose design. Therefore, modern lifting bodies are developed favouring a seamless integration between the different aerodynamic surfaces.
Several examples of lifting bodies were developed in the past. The Northrop HL-10 was built from NASA to evaluate the aerodynamic performance of a so called *inverted airfoil* configuration [1]. The HL-10 test bed was designed with a delta-planform lifting-body featuring three vertical planes, equipped with control surfaces [3]. HOPE-X is another example of Shuttle-like spacecraft. A 25% scale model of HOPE-X was released at an altitude of 20–30 km, by a stratospheric balloon and performing different manoeuvres [5]. Similar tests drove to FALKE program aimed at flying a sub-scale model of the Space Shuttle orbiter in real conditions [6].
The NASA HL-20 project resumes American efforts for the design of a crew emergency vehicle for ISS and used for crew rescue back to Earth [3]. Longitudinal manoeuvrability is allowed by two body flaps at fuselage trailing edge, while two canted fins are mounted on the aft portion of the model for lateral-directional control [7, 8].
Two main projects resume European efforts toward the experimental high-lift flight activities carried out in preparation of future space programs, namely Phoenix and IXV [9, 10]. The IXV vehicle was developed by ESA in order to test manoeuvring capabilities of a lifting body within a typical LEO re-entry environment. The Boeing X-37B is a unmanned vehicle currently operative that is the only one that re-enters from space, thus performing a horizontal landing on runway [8].
Finally, Dream Chaser (jointly designed by NASA and SNC) featuring a lifting-body aeroshape with small wings, is one of the most interesting design candidate vehicle up to now. It allows gliding, banking and landing to assigned conventional runways due to its good aerodynamic performances.
The Dream Chaser blunt nose-profile and flat bottomed shape represents an example of an accurate synthesis of all aerodynamic features needed to perform a safe re-entry.
As emerges from the addressed lifting body configurations, design of new-generation vehicles is a multidisciplinary task and, typically, requires an answer to antithetical design requirements. This category of design procedures is formulated as a multi-objective, multi-level, and Multi-disciplinary Design Optimization (MDO) procedure. Usually, a parametric shape generator efficiently supports a chain of sub-discipline analyses to an optimization procedure often performed with evolutionary algorithm (i.e., Genetic Algorithm, GA) [11, 13, 12].
In this framework, the paper explores two phases devoted to a design synthesis of a new spacecraft candidate for a return mission from Low Earth orbit (LEO), able to perform a landing on a horizontal conventional runway. Specifically, MDO is first adopted to determine design candidate configurations which adhere to a set of mission constraints. Furthermore, the support of Computational Fluid Dynamics (CFD) simulations to design synthesis is shown to refine the aerodynamics of the Phase-A compliant configuration.

2. Mission requirement and aeroshape conceptual configuration

The reference mission, pictorially shown in Figure 1, considers a concept aeroshape that possibly is put into LEO orbit by a launcher. Once in orbit, it can dock or undock on/from the ISS and perform an Earth re-entry. The CRV can be used either as emergency vehicle or simply as return vehicle for crew turnover on the ISS.
Initial Re-entry altitude and speed are set equal to $120\ Km$ and $7830\ m/s$, respectively. The admissible re-entry corridor is bounded by several constraints: maximum heat flux limit $Q_{max} \leq 760\ kW/m^2$; maximum dynamic pressure $q_{max} \leq 14\ kPa$; maximum normal load factor $2.5\ g$; maximum landing velocity $V_{max} \leq 110\ m/s$. The initial re-entry AoA, α_{opt}, is constrained to be within the range [35°, 50°]. The bank angle is assumed as a design variable, but no modulation of μ_a is assigned, and its value is constrained between the range [-50°, 50°].

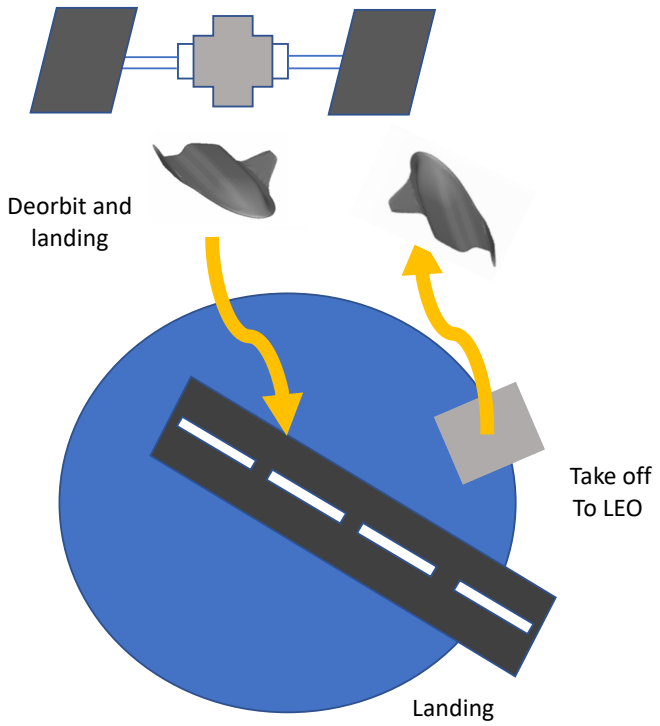

Figure 1 – Pictorial representation of a typical mission environment.

Finally, a maximum horizontal landing speed of $V_{max} = 110$ m/s is assumed as further design constraint. As the vehicle has to be intended as fully re-usable, it should perform a very long gliding trajectory.
Figure 2 regroups the steps of design framework. In the first step, an optimization procedure is used to build from scratch a conceptual configuration. The MDO procedure performs explorative evaluations of the configurations search domain, defined by the parametric variation of a state vector due to geometric, aero-thermodynamic, and flight dynamics suggestions [14].
In the conceptual phase, aerodynamic coefficients are computed with multi-regime Panel Methods (PMs).
Next, several simplifying assumptions made in the first level of design are progressively removed. Once the concept candidate has been individuated, the aeroshape configuration is frozen.
Phase-A design is represented by CFD simulations that are performed and used to assembly an accurate test matrix which refines the vehicle re-entry corridor. Furthermore, the addition of four functionally independent body flaps to the concept windside complete the low-speed design.
Mandatory information about the longitudinal stability margin at hypersonic and supersonic speeds are then obtained by CFD computations. Therefore, excursion of the center of gravity is addressed to find trim conditions which represents a prescription for vehicle flyability, as detailed in Ref.[15].
Moreover, a low-speed evaluation of vehicle Aerodynamics at landing incidence is also performed in pre- and post-stall conditions to evaluate efficiency of the preliminary configuration, as discussed in Reference [15], [16].
Subsequently, a prescribed Guidance Law (GL) expressed as a functional relation between the AoA, α, and the Mach number, M_∞, is derived using a single objective optimization procedure.

3. Shape Modelling

As remarked CRV design requires tools with a high level of efficiency and accuracy. To be compliant with optimization procedure, the shape model should allow local modifications, without altering the overall shape.
Without going into details of the shape model, we remark that the mesh arrangement over the CRV surface is obtained with no NURBS support surface: a three-dimensional parametric wireframe (see Fig. 3a-b) drives a self-organized cloud of points.

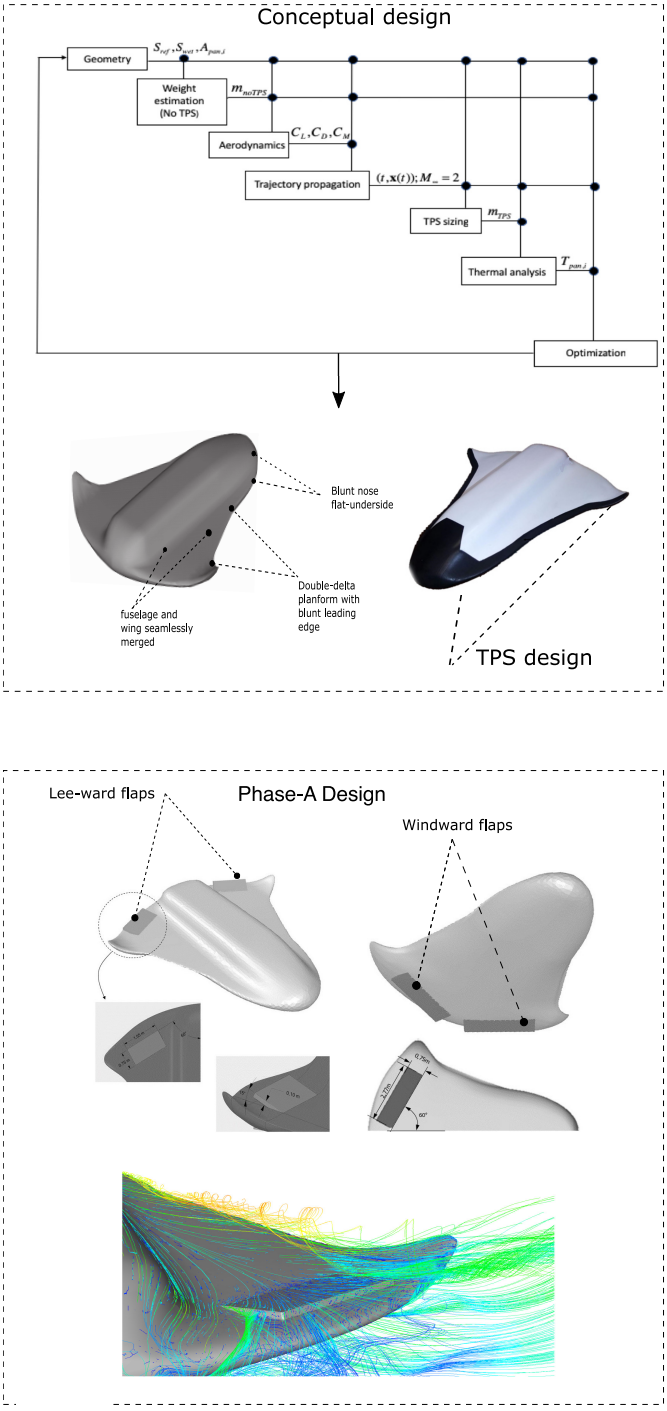

Figure 2 – Design framework: conceptual design (top); Phase-A design (bottom).

The sub-steps (S, I, A, G) of the shape generation procedure are shown in Fig. 3a-c. A uniform sampling S (Fig. 3-b) of points is performed on a set of master cross-sections selected over the wireframe. Wireframe parameters define the change of morphology.
Finally, a panel mesh formed by a quadrangular/triangular panels is generated from points representing the vehicle surface (obtained by a linear interpolation between wireframe cross-section), and a subsequent linear stretching A of sampled points (Fig.3-c) [14]).
In such a framework, the parametric model describes a transformation that properly remaps the search space into consistent configurations. Control parameters, allow a wide range of shape variations to handle properly different design objectives to meet (thermal or dynamical) constraints for the re-entry mission.

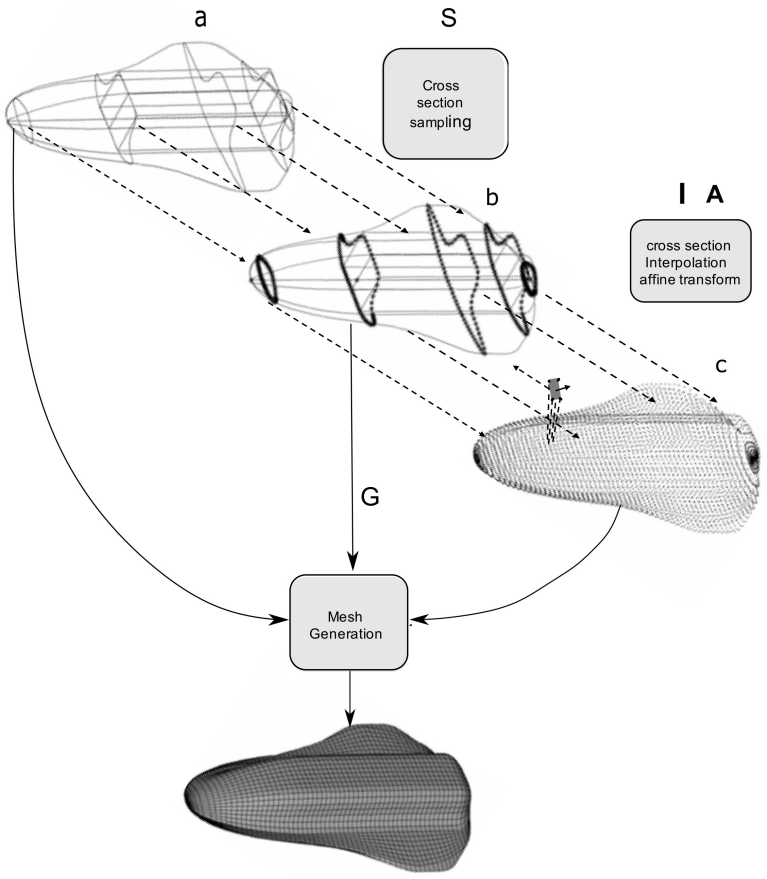

Figure 3 – Example of grid generation. a: wireframe; b: cross section sampling; c: point interpolation; d: panel mesh.

Consequently, such procedure features a seamless integration of different morphologies, rather than a mere superposition of different geometric entities. Grid topology ensures a topologically invariant shape Refs. [14], [18].

4. Optimal configuration

The optimization problem is resumed in the following table:

Objective function	Type
Mass	min
Cross-range	max
Constraints	**Range**
Dynamic pressure	$0 < q_{max} \leq 14$ KPa
Normal load	$0 < n_{zmax} \leq 2.5$
Touchdown speed	$0 < V_{tdmax} \leq 110$ m/s
Int. Temp	$T_{Int} \leq 0$
Ext. Temp	$T_{Out} \leq 0$

Table 1 – Optimization: objective functions and constraints.

A feasible non dominated candidate, resulting from the previous optimization is chosen having: $l_t = 9.25\ m$ (total length); $h = 1.5\ m$ (total height); $h_{ws} = 4.3\ m$ (half wing-span); $r_n = 0.469\ m$ (nose radius); $\theta = 40^\circ$ (bent angle), and is shown in Fig. 4. Mass budget provided the following estimations: 36 % for structure and mechanisms, 43 % for subsystems, 17% for TPS, and 4% for crew. According

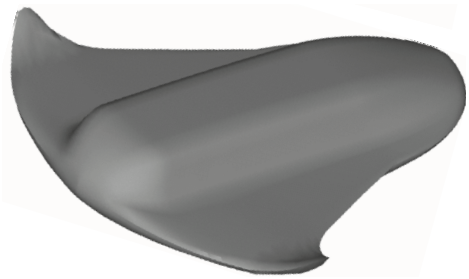

Figure 4 – Example of optimal aeroshape configuration.

to this decomposition the total spacecraft mass reads $m_{tot} = 12105\ kg$.

5. Phase-A design

5.1 High-speed Aerodynamic design

The Phase-A design of the present CRV takes advantage of several aerodynamic validations for the conceptual aeroshape assessment. With this in mind, an aerodynamic test-matrix having flight conditions individuated by (α, M_∞) values given by the arrays: $M_\infty = [2:25]$ and $\alpha = [0:40^\circ]$ is considered to feed a CFD simulation campaign. Conceptual aerodynamic evaluations by PM are validated with 3-D Eulerian CFD simulations, as shown in Fig. 5. High-speed Aerodynamics, is discussed in detail in Ref.[15].

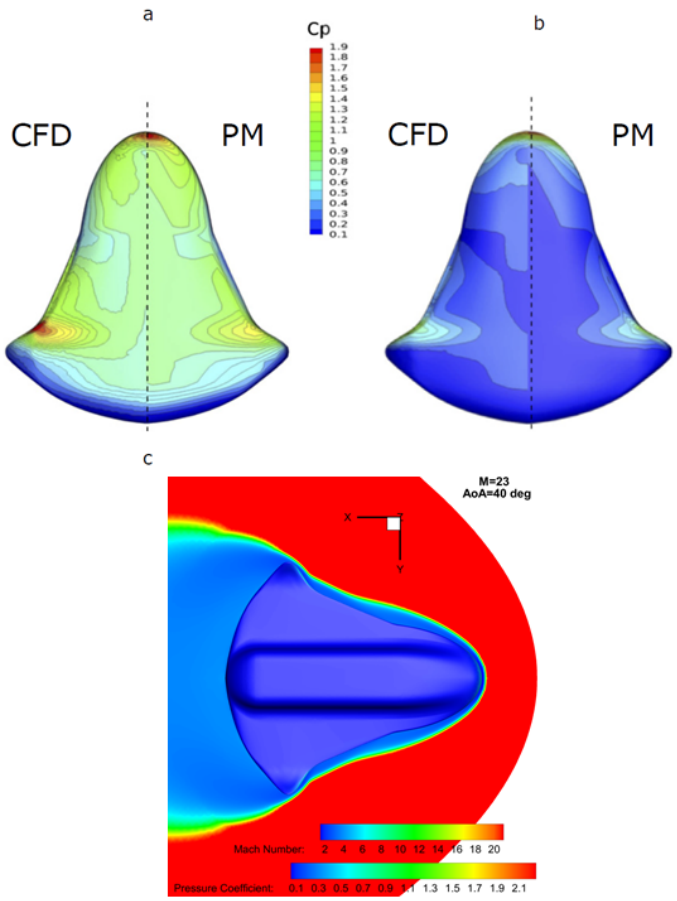

Figure 5 – Pressure contours obtained with CFD (left half) vs PM simulation (right half) at $M_\infty = 23$ (a) and $M_\infty = 2$ (b); pressure and Mach contours over the vehicle and a planform plane at $M_\infty = 23$ (c).

In Figure 5 simulations of the optimal concept aeroshape related to different attitudes i.e., ($M_\infty =$

$23,\ \alpha = 40°$) and ($M_\infty = 2,\ \alpha = 10°$) respectively, are shown and compared with results obtained by using PMs. CFD and PM results compare rather well over the vehicle surface. A slight pressure undershoot with PM near the winglet bending region is observed.
In Figure 6, lift and drag coefficients versus AoA, α, are provided for $M_\infty = 2$, 10, and 23.

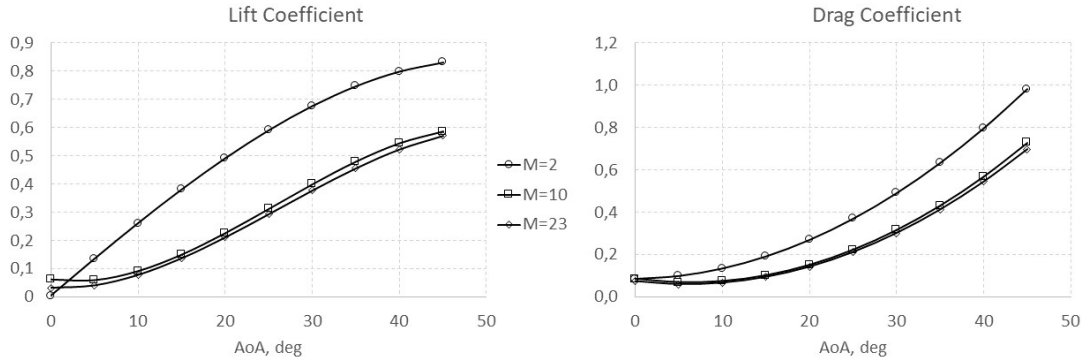

Figure 6 – Vehicle lift and drag coefficients vs α for $M_\infty = 2$, 10, and 23.

An aerodynamic database that is accessed via bi-linear interpolation/extrapolation by the trajectory integration code, allows to compute flight attitudes during re-entry to Earth.
To address the effects of high-temperature real-gas effects, e.g., vibrational excitation, dissociation and ionization (if any) of air, reacting flowfield simulations are carried out by means of several CFD computations [20]. For instance, Fig.7 provides contours of O_2 and N_2 mass fractions for $M_\infty = 19$, $H = 66.6\ km$ and $\alpha = 32°$. The chemical kinetics model of Park is adopted. [21]. A very thin shock

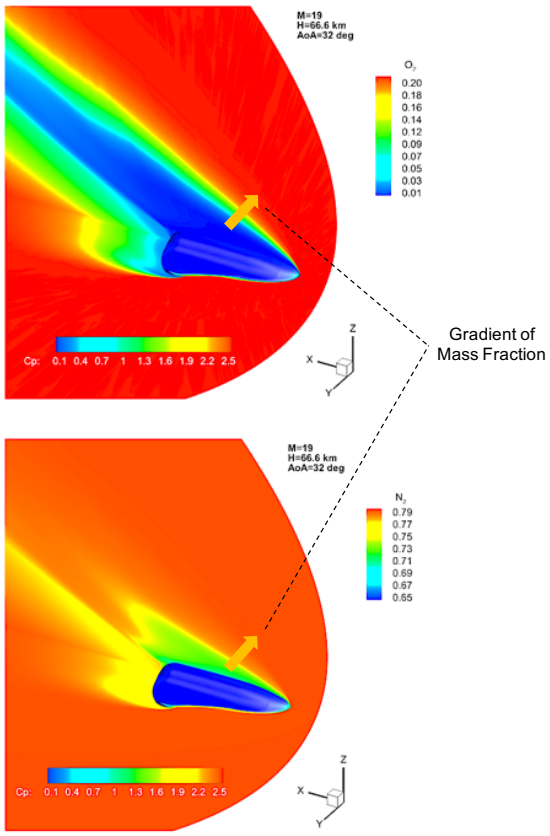

Figure 7 – Contours of O_2 and N_2 mass fractions for $M_\infty = 19$, $H = 66.6\ km$ and $\alpha = 32°$.

layer can be appreciated looking at at the dissociation levels in Figure 7. As it shown molecular Oxy-

gen is completely dissociated while N_2 just started dissociation.
To obtain an aerothermal environment compatible with a reusable thermal protection system (TPS), the vehicle should perform a very long gliding trajectory (of hour order magnitude) that slowly decelerates the spacecraft at high altitude.
This re-entry strategy can be pursued by flying at small flight path angles ($\gamma \ll 1$) with an enhanced aeroshape aerodynamics. Following this concept, an optimization problem is formulated to search the optimal prescribed guidance law, expressed as a (α, M_∞) modulation, able to provide a rather constant heat flux profile as longer as possible in the high-speed range.
The AoA modulation is formalised using a parametric functional dependence of the AoA with the Mach number, by using natural cubic splines.
A target figure corresponding to a maximum heat flux of $600\ kW/m^2$ is assigned, and initial entry conditions are given assuming $V_e = 7830\ m/s$, $\gamma_0 = -0.1°$. To perform a shallow re-entry reduces the drag-acceleration and obtain a constant value of heat flux in the most significant region of the re-entry corridor [17].

5.2 Low-speed Aerodynamic design

Aerodynamic analyses performed in low-speed regime shown that a BWB aeroshape with a delta wing planform conforms to the mission requirements and constraints. Furthermore, the current design also allows an efficient integration of body-flaps which improves vehicle control, trim and aerodynamic performances, especially for the landing phase.
Body-flaps, in fact, can be used either as elevon (i.e., symmetric deflections) or as ailerons (i.e., asymmetric deflections). Considering the configuration shown in Figure 8, the flap hinge line is positioned inboard with respect to the spacecraft trailing edge, to avoid a curved hinge line.

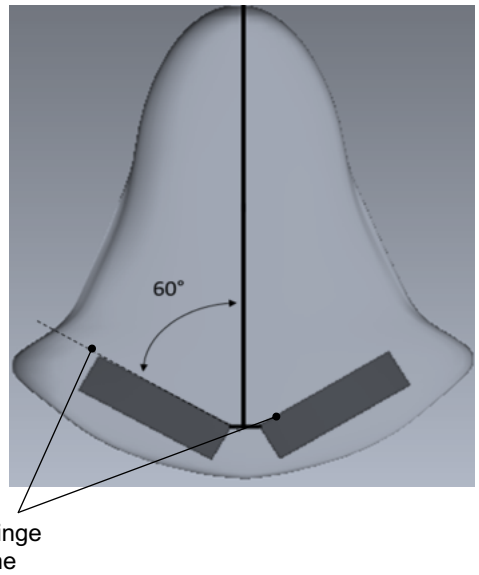

Figure 8 – Flap configuration over the wind-side.

Engineering-based approaches suggested $60°$ tilted hinge line of the flap to enlarge the region of the wing surface influenced by flap actuation (see Figure 8). The tilted hinge line, while deflecting the flap as aileron, allows also enough side force to promote rolling and yawing moments together with lift, drag, and pitching moment.
Aerodynamic performance at low speed is addressed with a steady state, RANS simulations performed in ANSYS Fluent by using the Shear-Stress Transport (SST) $\kappa - \omega$ model [19]. CFD simulations, are carried out at $M_\infty = 0.3$ that is the threshold limit which divides incompressible to compressible flows. For instance, pressure distributions over the spacecraft are shown in Figure 9. Aerodynamics at landing conditions is provided in terms of lift (C_L), drag (C_D), lift-to-drag ratio L/D, and pitching moments coefficient in Figure 10. The pole for moment reduction is fixed at 44,5% of the vehicle length, L.

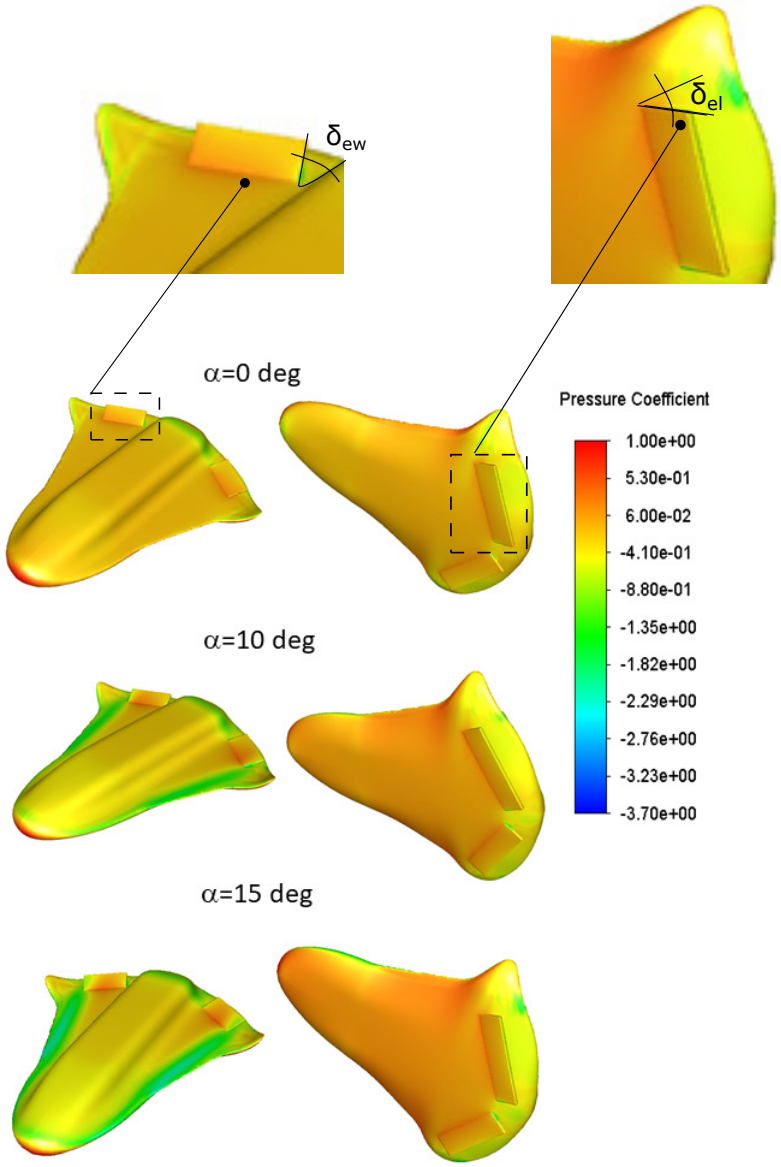

Figure 9 – Pressure surface distribution at $M_\infty = 0.3$ for $\alpha = 0, 10,$ and 15° with $\delta_{ew} = 10^\circ$, $\delta_{el} = 15^\circ$.

The Pohlamus analogy shows the different behaviour due to vortex lift contribution of C_L and C_D being

$$C_D = C_{D0} + C_L \cdot \tan\alpha \tag{1}$$

where C_{D0} the zero-lift drag coefficient.
Comparisons in Figure 10 show that the aeroshape having 10° windside elevon deflection together with 15° elevon leeside deflection has the same drag coefficients of the one having 10° windside elevon deflection alone (i.e., $\delta_{ew} = 10^\circ + \delta_{el} = 0^\circ$) in the AoA range from 4° to 12°. Slight differences in C_D arise at 0° and 15° AoA only.
On the other hand, remarkable differences are found among the other aerodynamic coefficients of these two flap settings by looking the lift coefficient, the pitching moment coefficient and L/D. For instance, the maximum aerodynamic efficiency when $\delta_{ew} = 10^\circ + \delta_{el} = 15^\circ$ is 25% larger than at $\delta_{ew} = 10^\circ + \delta_{el} = 0^\circ$ configuration.
Larger percentage differences exist for these two different flap settings while considering the pitching moment coefficients.

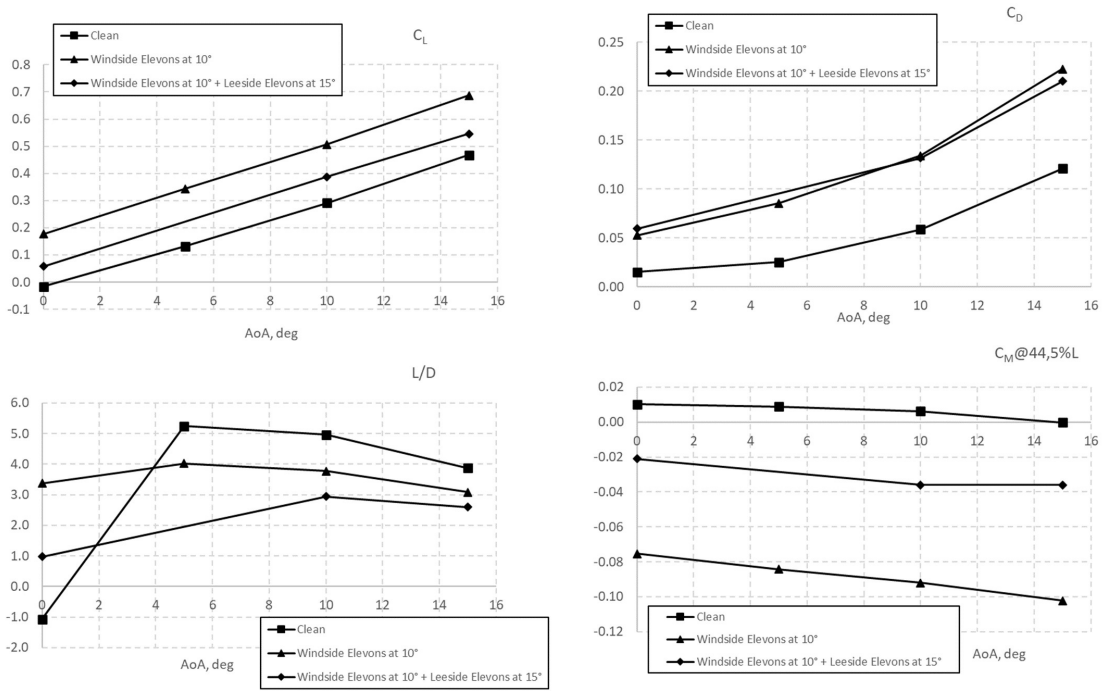

Figure 10 – Spacecraft Aerodynamics at landing conditions.

6. Conclusions

The paper dealt with a design procedure for a CRV vehicle aimed at performing a LEO return mission, which ends with a landing on an horizontal conventional runway. Conceptual design and Phase-A focused design were addressed in a preliminary design study. A multi-objective optimization procedure was used to find the conceptual configuration. CFD simulations performed on the optimal design candidate provided the necessary refinement of engineering evaluations with respect the boundaries of re-entry corridor. The optimized spacecraft has proven to be able to perform a trajectory characterized by a rather constant convective heat flux with a constraint value of 600 kW/m^2. It also has been shown the capability to horizontally land on a conventional runway at a touchdown speed below about 110 m/s, compatible with the structural limits of the landing gear.

7. Copyright Statement

The authors confirm that they, and/or their company or organization, hold copyright on all of the original material included in this paper. The authors also confirm that they have obtained permission, from the copyright holder of any third party material included in this paper, to publish it as part of their paper. The authors confirm that they give permission, or have obtained permission from the copyright holder of this paper, for the publication and distribution of this paper as part of the ICAS proceedings or as individual off-prints from the proceedings.

References

[1] Kempel R W, Painter W D and Thompson M O. *Developing and flight testing the HL-10 lifting body: A precursor to the space Shuttle.* NASA referece publication 1332, 1994

[2] Venel S, Fauncon P , Yanagihara M, Miyazawa Y, Akimoto T, and Sagisaka, M. *Hope-X high speed flight demonstration program phase II –a CNES/NAL/NASDA cooperation.* Advances in space research, 35, 1613–1616, 2003.

[3] Reed Dale R, and Lister D. *Wingless Flight: The Lifting Body Story.* University Press of Kentucky, 2002, ISBN 0-8131-9026-6.

[4] Marley C D, Driscoll J F. *Modeling an Active and Passive Thermal Protection System for a Hypersonic Vehicle.* AIAA SciTech Forum 9-13 January, Grapevine, Texas.

[5] Yanagihara M, Miyazawa Y, Munenaga T, Venel S, Guedron S, and Cretenet J C *Results of high-speed flight demonstration phase II.* Space Technology, 2005, 25(1), 37–50.

[6] Radespiel R. *Subsonic Flow Around US-Orbiter Model FALKE in the DNW.* AGARD Advisory Report No. 303, 1994.

[7] NASA, Human Space Flight. *Simulating Dream Chaser Spacecraft Aerodynamics: Subsonic through Hypersonic.* , 2020, https://www.nas.nasa.gov/SC19/demos/demo1.htmlprettyPhoto

[8] D Sziroczak and H Smith. *A review of design issues specific to hypersonic flight vehicles.* Progress in Aerospace Sciences, 84, 1-28, 2016.

[9] D Tumino and E Angelino and F Leleu, R Angelini and P Plotard and J Sommer. *The ESA Re-Entry System and Technologies Demonstrator Paving the Way to European Autonomous Space Transportation and Exploration Endeavours.* 59th International Astronautical Congress. IAC 2008. Glasgow, United Kingdom IAC 2008. Glasgow, United Kingdom.

[10] R Jategaonkar and R Behr and W Gockel and C Zorn. *Flight demonstrator concept for key technologies enabling future reusable vehicles.* AIAA Atmospheric Flight Mechanics Conference and Exhibition, 15-18 August 2005, San Francisco, California.

[11] D Dirkx and E Mooij. *Optimization of entry-vehicle shapes during conceptual design.* Acta Astronautica, 94(1) (2014) 198-214.

[12] M Tava and S Suzuki. *Multidisciplinary Design Optimization of a Re-Entry Vehicle Shape and Trajectory.* AIAA Paper 2001-28095, 2001.

[13] M A Lobbia. *Multidisciplinary Design Optimization of Waverider-Derived Crew Reentry Vehicles.* Journal of Spacecraft and Rockets, 54 (1) (2017) 233-245.

[14] Viviani A, Iuspa L, Aprovitola A. *Multi-objective Optimization for Re-entry Spacecraft Conceptual Design Using a Free-form Shape Generator.* Aerospace Science and Technology, 71, 312-324,2017.

[15] Viviani A, Iuspa L, Aprovitola A, Pezzella G. *Aeroshape design of reusable re-entry vehicles by multidisciplinary optimization and computational fluid dynamics.* Aerospace Science and Technology, 105, 2020.

[16] Viviani A, Aprovitola A, Pezzella G. *Low Speed Longitudinal Aerodynamics of a Blended Wing-Body Re-Entry Vehicle.* Aerospace Science and Technology, 107, 2020.

[17] A Aprovitola, N Montella, L Iuspa, Viviani A. *An optimal heat-flux targeting procedure for LEO re-entry of reusable vehicles.* Aerospace Science and Technology, Volume 112, May 2021.

[18] A Aprovitola, L Iuspa, Viviani A. *Thermal protection system design of a reusable launch vehicle using integral soft objects.* International Journal of Aerospace Engineering, 2019.

[19] *ANSYS Fluent User's Guide.*

[20] E Bucchignani and G Pezzella. *Computational flowfield analyses of hypersonic problems with reacting boundary layer.* Mathematics and Computers in Simulation, 81 (3), 656-669, 2010.

[21] A Viviani and G Pezzella and C Golia. *Effects of thermochemical modelling and surface catalyticity on an Earth re-entry vehicle.* Proceedings of the Institution of Mechanical Engineers, Part G: Journal of Aerospace Engineering, 225 (5), 523-540, 2011.